

Article

Synthesis of a Heterometallic [Zn₂Ca] Pinwheel Array Stabilized by Amide-Amide Synthons

Daniel Ejarque ¹, Teresa Calvet ², Mercè Font-Bardia ³ and Josefina Pons ^{1,*}¹ Departament de Química, Universitat Autònoma de Barcelona, Bellaterra, 08193 Barcelona, Spain² Departament de Mineralogia, Petrologia i Geologia Aplicada, Universitat de Barcelona, Martí i Franquès s/n, 08028 Barcelona, Spain³ Unitat de Difracció de Raig-X, Centres Científics i Tecnològics de la Universitat de Barcelona (CCiTUB), Universitat de Barcelona, Solé i Sabarís, 1-3, 08028 Barcelona, Spain

* Correspondence: josefina.pons@uab.es; Tel.: +34-935-812-895

Abstract: The rational design of heterometallic compounds bearing s-block metal ions have been a difficult task for chemists owing to their lack of preferential geometries. However, some strategies, such as the design of coordinating pockets with different sizes and/or donor atoms, have offered great results. In this work, this strategy has been tested using Ca(II) as an s-block metal ion and a compound previously obtained by our group with the formula [Zn₃(μ-ACA)₆(4-phpy)₂], which contains tetrahedral *N,O*- and octahedral *O*-coordinating pockets as a model structure. From this work, the corresponding heterometallic compound with the formula [Zn₂Ca(μ-ACA)₆(4-phpy)₂]-EtOH (**1**) has been successfully synthesized, and fully characterized, and its crystal structure has been elucidated. Furthermore, we have compiled all the crystal structures containing [Zn₂M] pinwheel secondary building units (SBUs), where M stands for an s-block metal ion, and the observed tendencies, as well as the promising applications as template SBUs for the preparation of 1D–3D coordination polymers, have been discussed. Finally, solid-state UV-Vis and photoluminescence have been recorded and compared with the homometallic [Zn₃(μ-ACA)₆(4-phpy)₂] compound.

Keywords: heterometallic complexes; trinuclear complexes; Zn(II); Ca(II); secondary building unit; X-ray crystal structure; α-acetamidocinnamic acid; solid-state photoluminescence



Citation: Ejarque, D.; Calvet, T.; Font-Bardia, M.; Pons, J. Synthesis of a Heterometallic [Zn₂Ca] Pinwheel Array Stabilized by Amide-Amide Synthons. *Inorganics* **2022**, *10*, 118. <https://doi.org/10.3390/inorganics10080118>

Academic Editors: Marius Andruh, Wolfgang Linert and Daniel García-Vivó

Received: 19 July 2022

Accepted: 12 August 2022

Published: 14 August 2022

Publisher's Note: MDPI stays neutral with regard to jurisdictional claims in published maps and institutional affiliations.



Copyright: © 2022 by the authors. Licensee MDPI, Basel, Switzerland. This article is an open access article distributed under the terms and conditions of the Creative Commons Attribution (CC BY) license (<https://creativecommons.org/licenses/by/4.0/>).

1. Introduction

Coordination compounds presenting diverse metal ions within the same molecule denoted as heterometallic complexes have recently received special attention owing to their superior structural versatility compared with their homometallic counterparts [1], as well as their unique physical and chemical properties arising from the synergistic effect of their different metallic ions [2,3]. As a result, this subclass of coordination complexes have been used in the fields of photoluminescence [4], magnetism [5], or catalysis [6], among others [7].

Researchers focused on heterometallic chemistry have been mostly devoted to the rational design of d-d and d-f metal complexes [8,9], while those presenting s-block metal ions have remained less explored caused by their challenging obtention [10]. This difficulty mainly arises from the larger atomic radii of s-block compared with d-block metals, which allows a broad range of coordination numbers and geometries for the s-block metals lack any geometrical preference [11–13]. One of the strategies that have successfully resulted in the obtention of d-s heterometallic compounds relies on the formation of different coordinating pockets within the same complex providing variable coordination environments and sizes where different metal ions can selectively bind [14,15]. Following this strategy and benefiting from the oxophilic character of s-block metal ions [16,17], the formation of four- and six-coordinating pockets based on *O*-donor or mixed *N,O*-donor atoms is a feasible way to selectively bind different metal ions toward the formation of

d-s heterometallic compounds [18–20]. Interestingly, the heterometallic arrays prepared by the aforementioned strategy can be utilized as secondary building units (SBUs) toward the formation of heterometallic 1D–3D coordination polymers (CPs) [21–23]. Accordingly, previous examples of d-s heterometallic SBUs with pockets of different sizes based in *N,O*- and *O*-donor atoms have been found in the literature [24–26].

In this context, we have been working on the synthesis of Zn(II) trinuclear pinwheel SBUs with $[Zn_3(\mu\text{-COO})_6]$ array based on the α -acetamidocinnamate (ACA) ligand. This SBU presents two different types of metal ions, displaying two lateral tetrahedral Zn(II) ions coordinated in *N,O*-based pockets, where the *N*-atom comes from non-sterically hindered pyridines (4-phenylpyridine, 4-phpy; 4,4'-bipyridine, 4,4'-bipy), while the central metal ions display an octahedral environment surrounded by oxygen atoms from six ACA moieties [27,28]. In addition, it has been observed that pinwheel SBUs are good candidates for the formation of heterometallic complexes owing to their inequivalent metal ions showing different coordination environments [29,30]. Furthermore, we have observed in previous contributions that pinwheel SBUs presenting ACA promote the formation of a pattern of amide-amide intramolecular interactions, which stabilize the pinwheel disposition as in other examples found in the literature, where the patterns can be formed by either H-bonds [28,31,32], or planar interactions [33,34]. Bearing in mind all the requirements stated above, we envisioned that the introduction of an s-block metal ion, such as Ca(II), should be selectively coordinated into the octahedral *O*-based pocket, forming a heterometallic SBU. Therefore, we have synthesized one $[Zn_2Ca]$ trinuclear compound with the formula $[Zn_2Ca(\mu\text{-ACA})_6(4\text{-phpy})_2]\cdot\text{EtOH}$ (**1**), which has been fully characterized. In addition, the crystal structure of $[Zn_2Ca(\mu\text{-ACA})_6(4\text{-phpy})_2]\cdot 2\text{EtOH}$ (**1C**) has been elucidated, revealing the pinwheel formation, as well as the introduction of the Ca(II) ions in the octahedral and the Zn(II) ions in the tetrahedral pocket. Finally, we have analyzed its solid-state UV-Vis and photoluminescence, and we have compared it with its homometallic counterpart.

2. Experimental Section

2.1. Materials and General Methods

Zinc(II) acetate dihydrate ($Zn(\text{OAc})_2\cdot 2\text{H}_2\text{O}$), calcium carbonate (CaCO_3), nitric acid 69% (HNO_3), α -acetamidocinnamic acid (HACA), 4-phenylpyridine (4-phpy) as reagents, and ethanol (EtOH) as solvent were purchased from Sigma-Aldrich. Calcium nitrate tetrahydrate $\text{Ca}(\text{NO}_3)_2\cdot 4\text{H}_2\text{O}$ was prepared using CaCO_3 and HNO_3 69% in a 1:2 molar ratio in Milli-Q water as solvent. Deuterated dimethylsulfoxide ($\text{DMSO-}d_6$) was used for the NMR experiments and was purchased from Eurisotop. All of them were used without further purification. All the reactions and manipulations were carried out in air at room temperature (RT). The powder X-ray diffraction (PXRD) pattern was measured with a Siemens D5000 apparatus with 40 kW and 45 mA using $\text{CuK}\alpha$ radiation with $\lambda = 1.5406 \text{ \AA}$. The diffractogram was recorded from $2\theta = 5^\circ$ to 30° with a step scan of 0.02° , counting 1 s at each step. Elemental analyses (C, H, N) were carried out on a Euro Vector 3100 instrument. HR-ESI-MS measurements were recorded after dissolving the corresponding complex in MeOH in a MicroTOF-Q instrument equipped with an electrospray ionization source (ESI) in positive mode. Na^+ ions come from the MeOH solvent which contains <50 ppb. Conditions were those used in routine experiments. The nebulizer pressure was 1.5 bar, the desolvation temperature was 180°C , dry gas was $6 \text{ L}\cdot\text{min}^{-1}$, the capillary counter-electrode voltage was 5 kV, and the quadrupole ion energy, was 5.0 eV. FTIR-ATR spectra were recorded on a Tensor 27 (Bruker) spectrometer, equipped with an attenuated total reflectance (ATR) accessory model MKII Golden Gate with a diamond window in the range $4000\text{--}500 \text{ cm}^{-1}$. ^1H , $^{13}\text{C}\{^1\text{H}\}$ and DEPT-135 NMR spectra were recorded on a Bruker Ascend 300 MHz spectrometer in $\text{DMSO-}d_6$ solutions at RT. All chemical shifts (δ) are given in ppm relative to Me_4Si as the internal standard. Solid-state UV-Vis spectra were carried out using a Cary 4000 spectrophotometer between 200–800 nm. Solid-state photoluminescence measurements were recorded using a Varian Cary Eclipse Fluorescence

spectrophotometer between 340 and 500 nm. CIE 1931 chromaticity diagram was generated using Origin Pro 2019b software.

2.2. Synthesis of $[Zn_2Ca(\mu-ACA)_6(4-phpy)_2]\cdot EtOH$ (**1**)

An EtOH solution (5 mL) of $Zn(OAc)_2\cdot 2H_2O$ (50.0 mg, 0.228 mmol) and $Ca(NO_3)_2\cdot 4H_2O$ (26.9 mg, 0.114 mmol) was carefully added to an EtOH solution (5 mL) of HACA (140 mg, 0.682 mmol) and 4-phpy (70.7 mg, 0.456 mmol) at RT. The solution was gently stirred for 15 h until a white precipitate was obtained, and the resulting powder was kept on ice for 1 h. Afterward, the reaction was filtered, washed with two portions of cold Et_2O (2×10 mL), and dried under vacuum, yielding **1**, which was characterized. Single crystals suitable for X-ray diffraction of $[Zn_2Ca(\mu-ACA)_6(4-phpy)_2]\cdot 2EtOH$ (**1C**) were obtained after letting evaporate the mother liquors at RT for 15 days.

1. Isolated Yield: 80.3 mg (40.2% based on Zn). Elemental analysis calc(%) for $C_{90}H_{84}N_8O_{19}Zn_2Ca$ (1752.53): C 61.68; H 4.83; N 6.39; found: C 61.55; H 4.54; N 6.36. HR-MS (ESI⁺, MeOH): m/z (%) = 156.0822 (100%) (calc. for $[4-phpy + H]^+$ = 156.0808); 228.0631 (100%) (calc. for $[HACA + Na]^+$ = 228.0631); 716.0806 (100%) (calc. for $[ZnCa(ACA)_3]^+$ = 716.0894); 943.1456 (100%) (calc. for $[ZnCa(ACA)_4 + Na]^+$ = 943.1452). FTIR-ATR (wave number, cm^{-1}): 3375(w) [$\nu(O-H)$], 3225(w) [$\nu(N-H)$], 3161–3003(br) [$\nu(C-H)_{ar} + \nu(C-H)_{alk}$], 2980–2650(br) [$\nu(C-H)_{al}$], 1667(m) [$\nu(C=O)$], 1652(w), 1599(s) [$\nu_{as}(COO)$], 1576(sh), 1523(m) [$\nu(C=C/C=N)$], 1491(w), 1447(w), 1386(s) [$\nu_s(COO)$], 1350(s) [$\delta(C=C/C=N)$], 1279(m), 1225(w), 1210(w), 1183(w), 1161(w), 1120(w), 1076(w) [$\delta_{ip}(C-H)$], 1031(w) [$\delta_{ip}(C-H)$], 1015(w) [$\delta_{ip}(C-H)$], 971(w), 964(w), 932(w), 837(w), 786(w), 760(m) [$\delta_{oop}(C-H)$], 730(w), 688(s) [$\delta_{oop}(C-H)$], 624(w), 609(w), 590(w), 574(m), 522(w). ¹H NMR (300 MHz; DMSO-*d*₆; Me₄Si; 298 K): δ = 9.14 [6H, s, NH_{ACA}], 8.65 [4H, dd, ³J = 4.6 Hz, ⁴J = 1.6 Hz, o-H_{py,4-phpy}], 7.81 [4H, m, o-H_{ph,4-phpy}], 7.73 [4H, dd, ³J = 4.6 Hz, ⁴J = 1.6 Hz, m-H_{py,4-phpy}], 7.51 [18H, m, o-H_{ACA} + m-H_{ph,4-phpy} + p-H_{ph,4-phpy}], 7.33 [12H, t, ³J = 7.4 Hz, m-H_{ACA}], 7.27 [6H, d, ³J = 7.4 Hz, p-H_{ACA}], 7.24 [6H, s, NH-C-CH_{ACA}], 4.35 [1H, t, ³J = 5.0 Hz, OH_{EtOH}], 3.44 [2H, qd, ³J = 6.9 Hz, 4.9 Hz, CH_{2,EtOH}], 1.96 [18H, s, CO-CH_{3,ACA}], 1.05 [3H, t, ³J = 7.0 Hz, CH_{3,EtOH}]. ¹³C{¹H} NMR (75 MHz; DMSO-*d*₆; Me₄Si; 298 K): δ = 170.3 [NH-CO_{ACA}], 168.4 [CO_{2,ACA}], 150.2 [o-C_{py,4-phpy}], 147.7 [Ph-C_{py,4-phpy}], 137.0 [Py-C_{ph,4-phpy}], 135.3 [O₂C-C_{ACA}], 129.9 [HN-C-CH-C_{ACA}], 129.6 [o-C_{ACA}], 129.4 [m-C_{ph,4-phpy}], 129.3 [p-C_{ph,4-phpy}], 128.6 [p-C_{ACA}], 128.4 [m-C_{ACA}], 128.1 [NH-C-CH_{ACA}], 127.0 [o-C_{ph,4-phpy}], 121.6 [m-C_{py,4-phpy}], 56.2 [CH_{2,EtOH}], 23.2 [CO-CH_{3,ACA}], 18.6 [CH_{3,EtOH}]. DEPT-135 NMR (75 MHz; DMSO-*d*₆; Me₄Si; 298 K): δ = 150.2 [o-C_{py,4-phpy}], 129.5 [o-C_{ACA}], 129.3 [m-C_{ph,4-phpy}], 129.3 [p-C_{ph,4-phpy}], 128.5 [p-C_{ACA}], 128.3 [m-C_{ACA}], 128.1 [NH-C-CH_{ACA}], 127.0 [o-C_{ph,4-phpy}], 121.5 [m-C_{py,4-phpy}], 56.1 [CH_{2,EtOH}], 23.2 [CO-CH_{3,ACA}], 18.6 [CH_{3,EtOH}].

2.3. X-ray Crystallographic Data

For compound **1C**, a colorless prism-like specimen was used for the X-ray crystallographic analysis. The X-ray intensity data were measured on a D8 Venture system equipped with a multilayer monochromator and a Mo microfocus ($\lambda = 0.71073$ Å). The frames of the compound were integrated with the Bruker SAINT Software package using a narrow-frame algorithm. All hydrogen atoms were refined using a riding model (AFIX) with an isotropic temperature factor equal to 1.2, the equivalent temperature factor of the atom to which are linked, and thus, the bond lengths of X-H were fixed.

The structure was solved and refined using the SHELXTL Software Package (version 2018/3) [35]. The final cell constants and volume were based upon refinement of the XYZ-centroids of reflections above 20 $\sigma(I)$. Data were corrected for absorption effects using the Multi-Scan method (SADABS). Crystal data and relevant details of structure refinement for **1C** are reported in Table 1. Complete information about the crystal structure and molecular geometry is available in CIF format via CCDC 2190605 (**1C**). Molecular graphics were generated with Mercury 4.3.1 software [36], using the POV-Ray image package [37]. The color codes for all of the molecular graphics are as follows: dark blue (Zn), light green (Ca), red (O), light blue (N), gray (C), and white (H). The accessible void volumes have

been calculated with Mercury 4.3.1 software [36], using a probe radius of 1.2 Å [38]. The evaluation of the geometry distortion of Zn(II) and Ca(II) cores of **1C** have been done using version 2.1 of SHAPE software from the corresponding cif files [39]. Hirshfeld surface analyses have been performed using CrystalExplorer 17.5 [40].

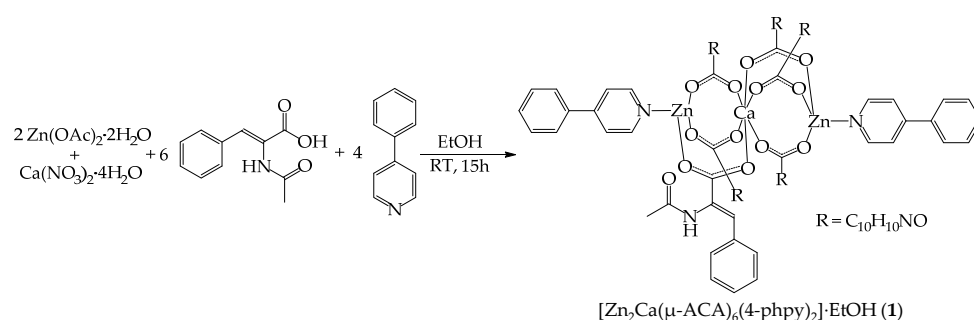
Table 1. Crystal data and structure refinement for **1C**.

	1C
CCDC	2190605
Empirical formula	C ₉₂ H ₉₀ CaN ₈ O ₂₀ Zn ₂
Formula weight	1798.53
T (K)	100(2)
Wavelength (Å)	0.71073
System, space group	Triclinic, P $\bar{1}$
Unit cell dimensions	
a (Å)	11.6745(12)
b (Å)	13.2064(13)
c (Å)	15.5353(16)
α (°)	67.641(3)
β (°)	85.612(4)
γ (°)	73.680(4)
V (Å ³)	2124.6(4)
Z	1
D _{calc} (mg/m ³)	1.406
μ (mm ⁻¹)	0.703
F (000)	938
Crystal size (mm ³)	0.243 × 0.115 × 0.048
hkl ranges	−16 ≤ h ≤ 16 −17 ≤ k ≤ 18 0 ≤ l ≤ 22
θ range (°)	2.221 to 30.593
Reflections collected/unique/[R _{int}]	13,031/13,031/[R _{int} = 0.0885]
Completeness to θ (%)	99.9
Absorption correction	Semi-empirical from equivalents
Max. and min. transmission	0.7461 and 0.6570
Refinement method	Full-matrix least-squares on F ²
Data/Restraints/Parameters	13,031/0/563
Goodness-on-fit on F ²	1.046
Final R indices [I > 2 σ (I)]	R ₁ = 0.0429, wR ₂ = 0.1153
R indices (all data)	R ₁ = 0.0900, wR ₂ = 0.1406
Extinction coefficient	n/a
Largest diff-peak and hole (e. Å ⁻³)	1.516 and −0.421

3. Results and Discussion

3.1. Synthesis and Characterization of **1**

Compound [Zn₂Ca(μ -ACA)₆(4-phpy)₂] \cdot EtOH (**1**) was prepared by combining Zn(OAc)₂ \cdot 2H₂O, Ca(NO₃)₂ \cdot 4H₂O, HACA, and 4-phpy in a 2:1:6:4 molar ratio using EtOH at room temperature (RT) (Scheme 1). The corresponding single crystals suitable for X-ray crystallographic analysis were obtained after allowing the mother liquors of the reaction to evaporate, yielding [Zn₂Ca(μ -ACA)₆(4-phpy)₂] \cdot 2EtOH (**1C**). Additional details of the synthesis and procedure for obtaining the single crystals are given in the Experimental Section.



Scheme 1. Outline of the synthesis of **1**.

The compound was characterized by powder X-ray diffraction (PXRD), elemental analysis (EA), HR-ESI-MS, FTIR-ATR, 1H , $^{13}C\{^1H\}$, and DEPT-135 NMR spectroscopies, and single crystal X-ray diffraction. The phase purity of the bulk sample of **1** was verified by PXRD (SI: Figure S1). In addition, the EA of compound **1** agrees with the proposed formula. The positive ionization mass spectrum (ESI⁺-MS) of the compound was recorded in MeOH as solvent. In these conditions, the complex displayed heterometallic fragments corresponding to $[ZnCa(ACA)_3]^+$ and $[ZnCa(ACA)_4 + Na]^+$ at m/z 716.0886 (100%) and 943.1456 (100%), respectively (SI: Figure S2). In the FTIR-ATR spectrum, the absence of a broad band between 2704 and 2405 cm^{-1} ($\nu(O-H)_{HACA}$) and a strong peak at 1637 cm^{-1} ($\nu(COOH)_{HACA}$) suggests that the HACA was not protonated. In addition, the spectrum presented the characteristic carboxylate bands at 1599 cm^{-1} for $\nu_{as}(COO)$ and 1386 cm^{-1} for $\nu_s(COO)$ (SI: Figure S3). The difference between these bands was 213 cm^{-1} due to a highly asymmetric bridged coordination mode [41,42], with a Δ value larger than its corresponding homometallic compound [27], in agreement with the data obtained from the crystal structure [41,43].

The 1H NMR spectrum was recorded to ascertain the ratio between the ACA and 4-ppy ligands, resulting in a 6:2 (ACA:4-ppy) molar ratio which agrees with the X-ray crystallographic data. It displayed a signal at 9.14 ppm corresponding to the NH proton atom of ACA, while the signals attributable to the aromatic protons of 4-ppy were observed between 8.65 and 7.51 ppm, some of them being overlapped with the *o*-H atoms from ACA in the signal of 7.51 ppm. In addition, the remaining aromatic protons from ACA were observed at 7.33 and 7.24 ppm, followed by the hydrogen atom from the alkene group, which appeared at 7.24 ppm. Finally, the signals observed in the upfield region corresponded to the EtOH hydrogen atoms at 4.35, 3.44, and 1.05 ppm, respectively, together with the methyl proton atoms at 1.96 ppm (SI: Figure S4) [44].

The $^{13}C\{^1H\}$ NMR displayed the characteristic bands of the carbonyl and carboxylate groups from ACA at 170.3 and 168.4 ppm, respectively (SI: Figure S5a). In addition, the signals corresponding to the carbon atoms from the 4-ppy appeared between 150.2 and 129.3 ppm. In this zone, the carbon atoms from the alkene group of ACA were also shown at 135.3 and 128.1 ppm, in line with the absence of the first band in the DEPT-135 spectrum (SI: Figure S5b). Furthermore, the aromatic carbon atoms from ACA appeared between 129.9 and 128.4 ppm, while the methyl carbon atom was found at 23.2 ppm. Finally, the upfield region of the spectra also contained two signals attributed to the EtOH carbon atoms (56.2 and 18.6 ppm) (SI: Figure S5a).

3.2. Structural Description and Hirshfeld Surface Analysis of **1C**

Compound **1C** belongs to the triclinic $P\bar{1}$ space group. It consisted of a heterometallic pinwheel array presenting two lateral Zn(II) and one central Ca(II) metal ions, as well as six ACA ligands with $\mu_2-\eta^1:\eta^1$ coordination modes that formed the trinuclear array, while two 4-ppy ligands occupied the apical positions (Figure 1a). The two Zn(II) lateral ions displayed $[ZnO_3N]$ cores with tetrahedral geometries ($S = 0.959$, $\tau_4 = 2.53$) [45,46], while the central Ca(II) ion formed a $[CaO_6]$ core with an octahedral geometry ($S = 0.100$,

$\text{ata} = 60^\circ$) (Table 2; SI: Table S1) [45,47,48]. Furthermore, the supramolecular structure of **1C** displayed voids with an accessible volume of 32.03 \AA^3 (1.5% of the unit cell volume) [38], where two EtOH molecules were situated. The bond lengths involving the Zn(II) metal center ranged between $1.9622(16)$ and $2.0504(19) \text{ \AA}$, while those with Ca(II) as metal *core* presented bond lengths oscillating between $2.2055(17)$ and $2.2117(18) \text{ \AA}$, giving rise to highly asymmetric bridged coordination modes, as the FTIR-ATR spectrum suggest. In addition, the bond angles ranged between $89.50(7)$ and 180° . All of these values are similar to other heterometallic pinwheel arrays containing lateral Zn(II) and central Ca(II) metallic centers [49,50].

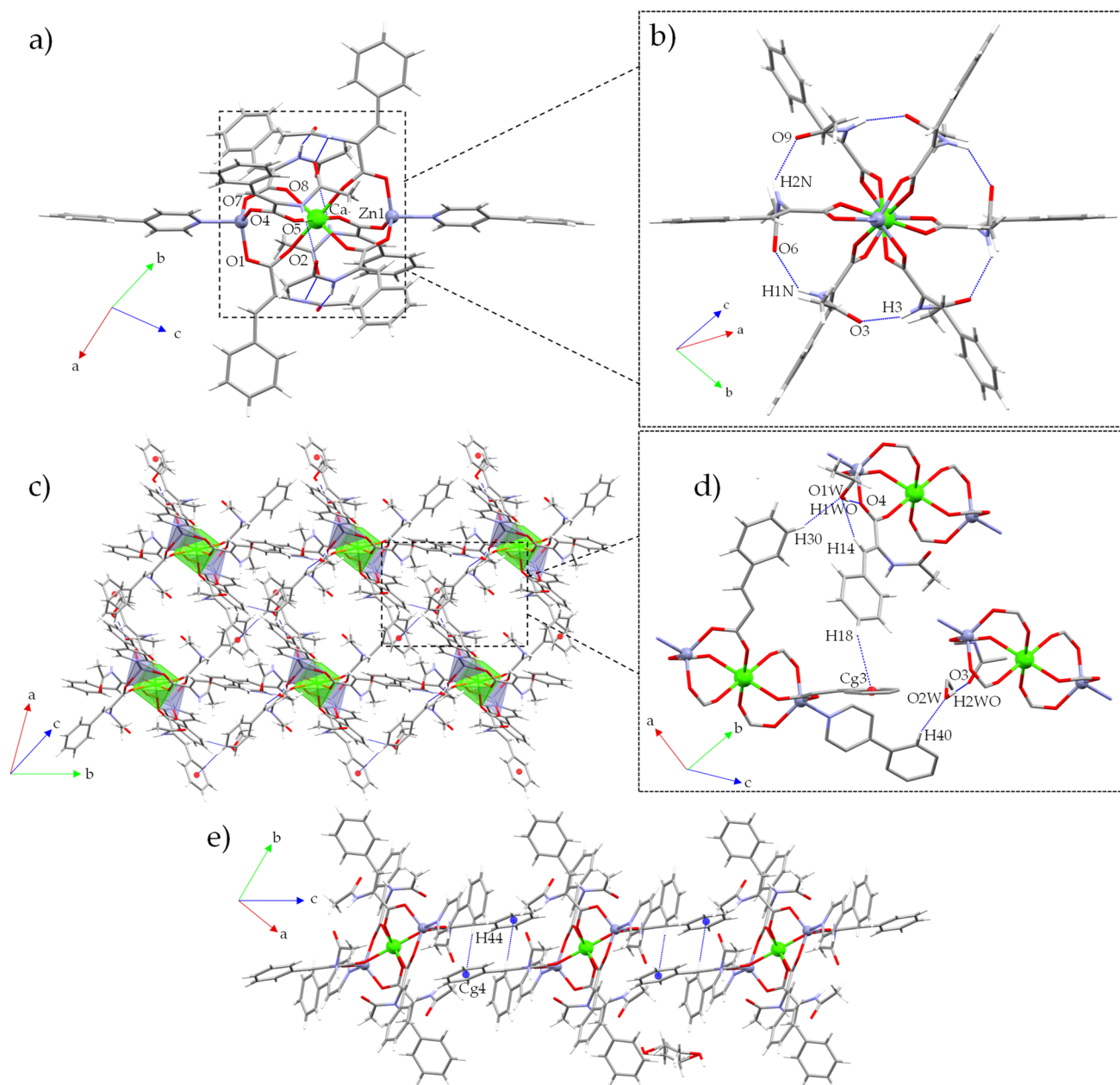


Figure 1. (a) Molecular structure of compound **1C**. (b) Intramolecular interactions (c) Supramolecular expansion of **1C** along the (002) plane. (d) In-detail view of the intermolecular interactions involved in the expansion along the (002) plane of **1C**. (e) General view of the supramolecular expansion of **1C** through the [001] direction.

Table 2. Selected bond lengths (Å), bond angles (°), intramolecular and intermolecular interactions (Å) for compound **1C**.

Bond Lengths (Å)				
Zn(1)-O(1)	1.9622(16)	Ca-O(2)	2.2115(17)	
Zn(1)-O(4)	1.9626(17)	Ca-O(5)	2.2117(18)	
Zn(1)-O(7)	1.9375(16)	Ca-O(8)	2.2055(17)	
Zn(1)-N(4)	2.0504(19)			
Bond Angles (°)				
O(1)-Zn(1)-O(4)	110.43(7)	O(2)-Ca-O(5)#1	93.98(7)	
O(1)-Zn(1)-N(4)	102.87(7)	O(5)-Ca-O(5)#1	180.0	
O(4)-Zn(1)-N(4)	100.42(7)	O(8)-Ca-O(2)	88.09(6)	
O(7)-Zn(1)-O(1)	123.72(7)	O(8)-Ca-O(2)#1	91.91(6)	
O(7)-Zn(1)-O(4)	117.39(8)	O(8)-Ca-O(5)	89.50(7)	
O(7)-Zn(1)-N(4)	96.16(7)	O(8)-Ca-O(5)#1	90.50(7)	
O(2)#1-Ca-O(2)	180.0	O(8)-Ca-O(8)#1	180.0	
O(2)-Ca-O(5)	86.02(7)			
Twist Angles (°)				
O(2)#1-Cg(1)-Cg(2)-O(5)#1	58.08	O(5)-Cg(1)-Cg(2)-O(8)#1	61.97	
O(8)-Cg(1)-Cg(2)-O(2)	59.95			
Intramolecular Interactions (Å)				
D-H...A	D-H (Å)	H...A (Å)	D...A (Å)	>D-H...A (°)
N(1)-H(1N)...O(6)	0.88	1.99	2.826(3)	158
N(2)-H(2N)...O(9)	0.88	2.13	2.840(2)	137
N(3)-H(3)...O(3)	0.88	2.17	2.892(3)	140
Intermolecular Interactions (Å)				
D-H...A	D-H (Å)	H...A (Å)	D...A (Å)	>D-H...A (°)
O(1W)-H(1WO)...O(4)	0.84	2.07	2.903(5)	173
O(2W)-H(2WO)...O(3)	0.84	2.24	3.053(5)	162
C(14)-H(14)...O(1W)	0.95	2.52	3.439(5)	162
C(30)-H(30)...O(1W)	0.95	2.48	3.390(6)	161
C(40)-H(40)...O(2W)	0.95	2.42	3.293(5)	152
C(18)-H(18)...Cg(3)	0.95	3.05	3.791(5)	136
C(44)-H(44)...Cg(4)	0.95	3.13	3.920(5)	142

#1: -x+1, -y+1, -z+1. Cg(1) = O(2)#1 O(5) O(8); Cg(2) = O(2) O(5)#1 O(8)#1; Cg(3) = C(4) C(5) C(6) C(7) C(8) C(9); Cg(4) = C(15) C(16) C(17) C(18) C(19) C(20)

The intramolecular interactions of **1C** were based on a hexagonal pattern of amide...amide homosynthons [51], presenting three different pairs of N-H...O interactions as their different contributions of H...O and O...H contacts indicated in their respective 2D fingerprint plots (SI: Figure S6). This pattern has been previously observed by our group, stabilizing the structure of similar complexes presenting pinwheel arrays (Figure 1b) [27,28]. On the other side, their intermolecular interactions propagated the structure along the (002) plane through their occluded EtOH molecules, which join together contiguous pinwheel arrays by H-bonds, involving the hydroxyl groups of the EtOH molecules and the carbonyl and carboxylate oxygen atoms from ACA, as well as three complementary C-H...O interactions formed by the oxygen atoms of the EtOH molecules and nearby hydrogen atoms of either ACA or 4-ppy ligands. All these interactions were clearly highlighted in the Hirshfeld surface of **1C** as red spots, representing either the O...H or H...O contacts, with a 4.7% of the contact surface, where the O...H contacts show closer interactions compared with the H...O contacts (SI: Figure S7a,b). In addition, this propagation was also supported by C-H... π interactions between two ACA ligands of nearby trinuclear units, which were also observed in the curvedness representation of the Hirshfeld surface of **1C**, representing a 17.1% contact surface in the 2D fingerprint plots, and displaying the characteristic wings shape (Figure 1c,d; SI: Figure S7c,d) [52]. Finally, the structure was also expanded through the [001] direction by reciprocal C-H... π interactions between *o*-H atoms from 4-ppy and vicinal ACA ligands, giving rise to a 3D net (Figure 1e).

3.3. CSD Study of Heterometallic $[Zn_2M]$ Pinwheel SBUs ($M = s$ -Block Metal)

A search in the Cambridge Structural Database (CSD version 5.43 March 2022) of $[Zn_2M]$ pinwheel SBUs, where M stands for an s -block metal ion, revealed a total of 35 hits. The synthetic methodologies followed mainly used nitrate salts as metal sources, while MCl_2 , $M(OH)_2$, and $Zn(OAc)_2 \cdot 2H_2O$ were used to a lesser extent. It also has been noticed that polar solvents, such as H_2O , $EtOH$, or DMF , have been used in all the syntheses. In addition, for the preparation of 27 complexes, high temperatures (over $80^\circ C$) and long reaction times (over 48 h) were required. Conversely, our compound was obtained in mild conditions, using $EtOH$ as the solvent at RT. Of note, some examples were found where the preparation of these SBUs was performed starting from a pre-synthesized complex containing pivalate [53,54] or crotonate [55,56] ligands. Interestingly, compound $\{[Zn_2Ca(fda)_4] \cdot 2Me_2NH_2\}_n$ ($fda = 2,5$ -furandicarboxylate) was synthesized from a pre-formed 0D pinwheel SBU using pivalate and pyridine, which preserved its trinuclear array when their pivalate ligands were exchanged with 2,5-furandicarboxylates toward the formation of a 3D CP [54]. (SI: Table S2).

The results of the CSD search are summarized in Figure 2 and the SI (Table S3). It was observed that 19 structures showed a central Ca(II) ion, followed by Mg(II) displaying 5 hits, Na(I) with 4 hits, Sr(II) and Ba(II) both presenting 3 hits, and K(I) containing 1 hit. Furthermore, complexes displaying 0D (11 hits) and 3D (14 hits) structures were more abundant than 1D or 2D CPs (both presenting 5 hits). Of note, the central s -block metal ions were located in octahedral O -based pockets in almost every structure, except for three examples containing Sr(II) or Ba(II), whose bigger ionic radii allowed the expansion of the coordination sphere reaching $[SrO_8]/[BaO_8]$ cores [15,57,58]. Otherwise, the coordination sphere of the lateral Zn(II) ions showed diverse coordination pockets, displaying $[ZnO_4]$ (15 hits), $[ZnO_5]$ (1 hit), $[ZnO_3N]$ (13 hits), $[ZnO_4N]$ (4 hits), and $[ZnO_3N_2]$ (2 hits) cores. However, the five-coordinated environments were relatively scarce, being mainly originated from μ_2 - η^2 : η^1 carboxylate coordination modes [22,56,59,60], the coordination of water molecules [61,62], or by μ_2 - η^2 ditopic oxygen atoms from carboxylate moieties [63] (SI: Figure S8). Regarding the tetrahedral pockets, the two cores found differed in their lateral position, which could be either a N - or an O -atom. In 12 structures presenting $[ZnO_3N]$ cores, the N -atoms arose from pyridine or bipyridine ligands displaying 0D or 1D complexes, such as in **1C**. At the same time, there was a unique case where 2D sheets were formed by the expansion of a dicarboxylate ligand [64]. Conversely, all the structures with $[ZnO_4]$ cores displayed 2D or 3D arrays, showing mostly solvent molecules coordinated to their apical positions, while only in three examples the molecular expansion was done by both the carboxylates forming the SBU and those located in their apical positions [15,54,65]. Therefore, this overview showed that while the investigation regarding heterometallic complexes with $[Zn_2M]$ ($M = s$ -block metal ion) pinwheel SBUs has been scarce, it offers a great structural variability toward the formation of heterometallic arrays which are completely modulable, as it is possible to extend their structures through their apical positions or their central ligands either by bipyridines, carboxylates, or both. However, this compilation shows that further investigation about this SBU needs to be carried out to control the obtained structures.

3.4. Photophysical Properties

The solid-state UV-Vis and photoluminescence of **1** and $[Zn_3(ACA)_6(4\text{-phpy})_2]$ was recorded (Figure 3). The absorption spectra of both compounds showed similar profiles, presenting a broad unstructured signal with a maximum between 240 and 323 nm (**1**), and 240 and 330 nm ($[Zn_3(ACA)_6(4\text{-phpy})_2]$). When irradiated at an excitation wavelength of 320 nm, both compounds showed one unstructured signal with its maxima centered at 360 nm and a Stokes shift of 3472 cm^{-1} , suggesting local electronic transitions which have been tentatively attributed to intra-ligand charge transfers (ILCT) of either the ACA or the 4-pphy ligands [66,67]. The comparison between the two compounds showed that they only present minimal differences between their emission profiles. In addition, the resultant

emission color for both compounds was blue for **1** and electric violet for the homometallic compound, according to the CIE 1931 chromaticity diagram (SI: Figure S9) [68]. Therefore, it was observed that the exchange of a Zn(II) for a Ca(II) in the central position of the pinwheel SBU did not confer significant differences to the photoluminescence properties of these complexes.

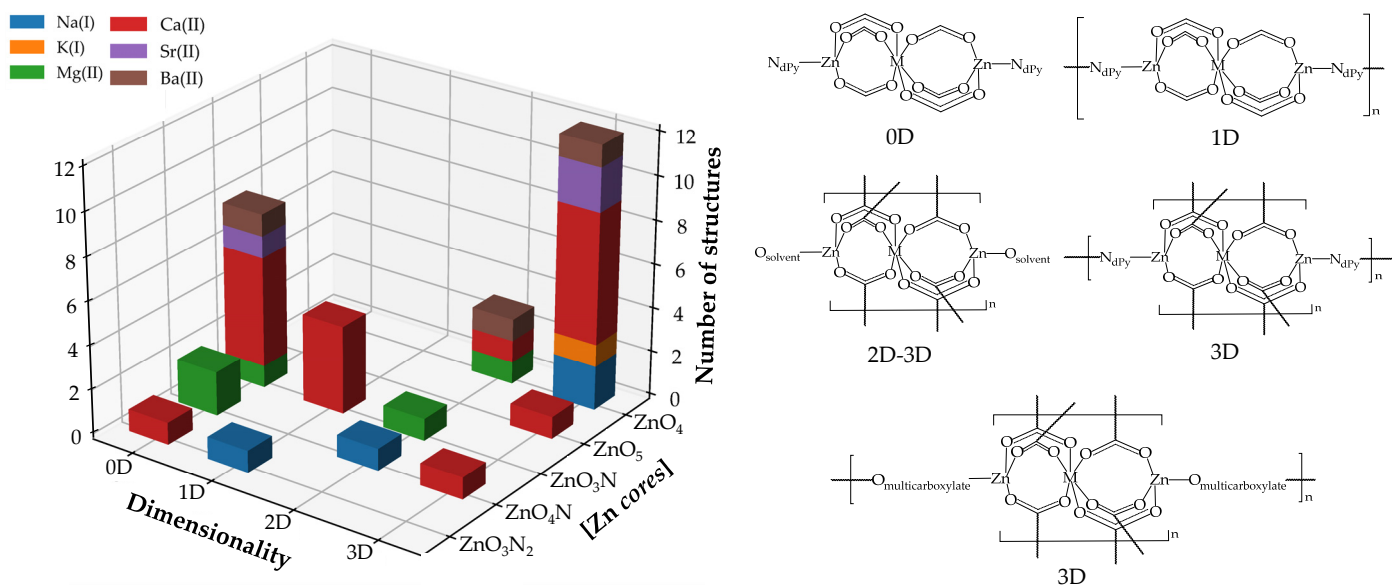


Figure 2. Results of the CSD study of $[Zn_2M]$ pinwheel SBUs ($M = s$ -block metal ion) with a representation of the more abundant type of structures.

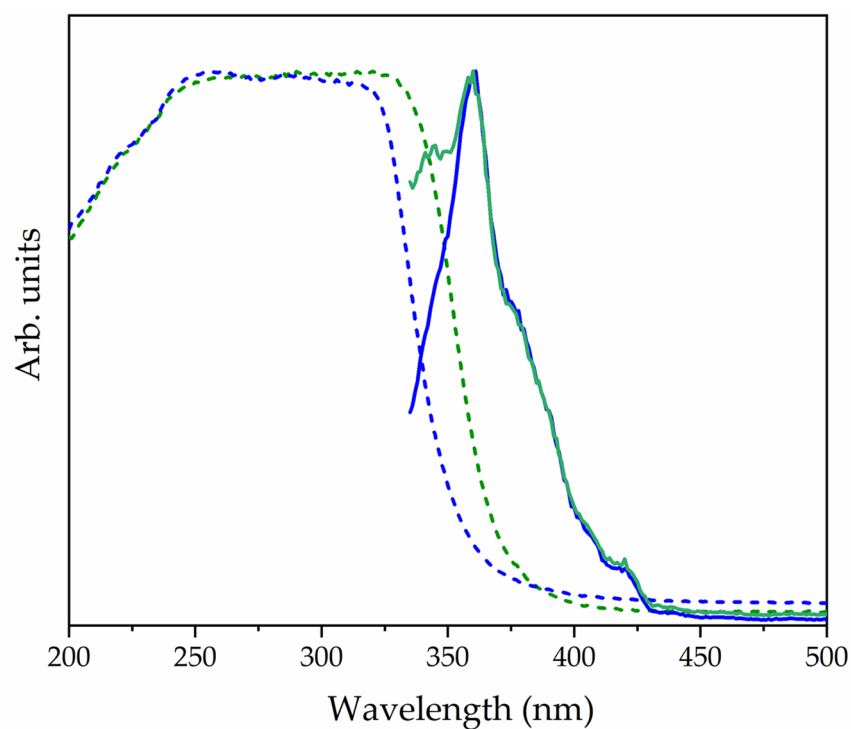


Figure 3. Normalized absorption (dashed line) and emission (solid line) spectra of compound **1** (green) and $[Zn_3(\mu\text{-ACA})_6(4\text{-phpy})_2]$ (blue).

4. Conclusions

In this contribution, we successfully synthesized and characterized one d-s heterometallic compound with a pinwheel array and formula $[Zn_2Ca(\mu\text{-ACA})_6(4\text{-phpy})_2]\cdot\text{EtOH}$ (**1**). This compound was obtained through the self-assembly of octahedral *O*- and tetrahedral *N,O*-based coordinating pockets that enable the selective coordination of Ca(II) and Zn(II) ions to the different coordination environments. The elucidation of the crystal structure **1C** confirmed the selective coordination between Zn(II)/Ca(II) through the formation of the aforementioned pockets. Furthermore, we compiled all the structures related to **1C** presenting s-block metal ions in the central pocket of the pinwheel, observing the most common synthetic conditions and the great versatility of this SBU. In addition, the solid-state UV-Vis and photoluminescence of **1** were recorded and compared with the corresponding homometallic compound and we observed that the substitution of a Zn(II) by a Ca(II) ion in the central octahedral pocket of the pinwheel SBU slightly altered both curve profiles. To conclude, the use of ACA presents a good option for the formation of heterometallic pinwheel SBUs using mild conditions compared with previously reported syntheses and presenting potential applications as a template for the preparation of extended networks using the pinwheel motif as a predetermined SBU.

Supplementary Materials: The following supporting information can be downloaded at: <https://www.mdpi.com/article/10.3390/inorganics10080118/s1>, Figure S1: PXRD patterns; Figure S2: ESI-MS fragments; Figure S3: FTIR-ATR spectrum; Figure S4: ¹H NMR spectrum; Figure S5: ¹³C{¹H} and DEPT-135 NMR spectra; Table S1: Geometric evaluation of the metal *cores*; Figures S6 and S7: Hirshfeld surface analysis; Table S2: Overview of the synthetic conditions utilized for synthesizing the complexes found in the CSD search; Table S3: Overview of the main SBU features of the complexes found on the CSD search; Figure S8: Outline of the five-coordinated Zn(II) *cores* found on the CSD search; Figure S9: CIE 1931 chromaticity diagram. References [69–75] are cited in the Supplementary Materials.

Author Contributions: Conceptualization, J.P.; methodology, D.E.; software, D.E.; validation, J.P. and T.C.; formal analysis, D.E. and M.F.-B.; investigation, D.E.; resources, J.P. and T.C.; data curation, D.E. and M.F.-B.; writing—original draft preparation, D.E.; writing—review and editing, J.P.; visualization, D.E.; supervision, J.P.; project administration, J.P.; funding acquisition, J.P. All authors have read and agreed to the published version of the manuscript.

Funding: This research was funded by the CB615921 project, the CB616406 project from “Fundació La Caixa”, and the 2017SGR1687 project from the Generalitat de Catalunya. D.E. acknowledges the PIF pre-doctoral fellowship from the Universitat Autònoma de Barcelona.

Institutional Review Board Statement: Not applicable.

Informed Consent Statement: Not applicable.

Data Availability Statement: Accession code 2190605 (**1**) contains the supplementary crystallographic data for this paper. These data can be obtained free of charge via www.ccdc.cam.ac.uk/data_request/cif, (accessed on 11 August 2022), or by emailing data_request@ccdc.cam.ac.uk, or by contacting The Cambridge Crystallographic Data Centre, 12 Union Road, Cambridge CB2 1EZ, UK; fax: +44 1223 336033.

Conflicts of Interest: The authors declare no conflict of interest.

References

1. Cruz, C.; Spodine, E.; Audebrand, N.; Venegas-Yazigi, D.; Paredes-García, V. Structural Versatility of 3d-Ce^{III} Heterometallic Coordination Polymers Using Co^{II} or Cu^{II}. *Cryst. Growth Des.* **2018**, *18*, 5155–5165. [[CrossRef](#)]
2. Garden, J.A.; Saini, P.K.; Williams, C.K. Greater than the Sum of Its Parts: A Heterodinuclear Polymerization Catalyst. *J. Am. Chem. Soc.* **2015**, *137*, 15078–15081. [[CrossRef](#)] [[PubMed](#)]
3. Ma, L.; Li, L.; Zhu, G. Platinum-containing heterometallic complexes in cancer therapy: Advances and perspectives. *Inorg. Chem. Front.* **2022**, *9*, 2424–2453. [[CrossRef](#)]

4. He, X.; Liu, Y.; Lv, Y.; Dong, Y.; Hu, G.; Zhou, S.; Xu, Y. L- and D-[LnZn(IN)₃(C₂H₄O₂)_n] (Ln = Eu, Sm, and Gd): Chiral Enantiomerically 3D 3d–4f Coordination Polymers Constructed by Interesting Butterfly-like Building. *Inorg. Chem.* **2016**, *55*, 2048–2054. [[CrossRef](#)] [[PubMed](#)]
5. Andruh, M. Heterotrimetallic complexes in molecular magnetism. *Chem. Commun.* **2018**, *54*, 3559–3577. [[CrossRef](#)]
6. Buchwalter, P.; Rosé, J.; Braunstein, P. Multimetallic Catalysis Based on Heterometallic Complexes and Clusters. *Chem. Rev.* **2015**, *115*, 28–126. [[CrossRef](#)]
7. Majumder, I.; Chakraborty, P.; Álvarez, R.; Gonzalez-Diaz, M.; Peláez, R.; Ellahioui, Y.; Bauza, A.; Frontera, A.; Zangrando, E.; Gómez-Ruiz, S.; et al. Bioactive Heterometallic Cu^{II}–Zn^{II} Complexes with Potential Biomedical Applications. *ACS Omega* **2018**, *3*, 13343–13353. [[CrossRef](#)]
8. Sakamoto, M. d-f Heteronuclear complexes: Synthesis, structures and physicochemical aspects. *Coord. Chem. Rev.* **2001**, *219–221*, 379–414. [[CrossRef](#)]
9. Chipman, J.A.; Berry, J.F. Paramagnetic Metal–Metal Bonded Heterometallic Complexes. *Chem. Rev.* **2020**, *120*, 2409–2447. [[CrossRef](#)]
10. Fromm, K.M. Chemistry of alkaline earth metals: It is not all ionic and definitely not boring! *Coord. Chem. Rev.* **2020**, *408*, 213193. [[CrossRef](#)]
11. Chen, Y.; Zheng, L.; She, S.; Chen, Z.; Hu, B.; Li, Y. Two novel heterometallic Cu^{II}–Sr^{II} coordination polymers based on 3,5-pyrazoledicarboxylic acid: Synthesis, crystal structures and magnetic properties. *Dalton Trans.* **2011**, *40*, 4970. [[CrossRef](#)] [[PubMed](#)]
12. Chen, Y.; She, S.; Gao, Q.; Gao, D.; Wang, D.; Li, Y.; Liu, W.; Li, W. Synthesis, structures and properties of the first series of Sr^{II}–M^{II} (M = Cu, Co, Ni and Zn) coordination polymers based on pyridine-2,5-dicarboxylic acid. *CrystEngComm* **2014**, *16*, 1091–1102. [[CrossRef](#)]
13. Zang, Y.; Li, L.-K.; Zang, S.-Q. Recent development on the alkaline earth MOFs (AEMOFs). *Coord. Chem. Rev.* **2021**, *440*, 213955. [[CrossRef](#)]
14. Fenton, H.; Tidmarsh, I.S.; Ward, M.D. Homonuclear and heteronuclear complexes of a four-armed octadentate ligand: Synthetic control based on matching ligand denticity with metal ion coordination preferences. *Dalton Trans.* **2009**, 4199. [[CrossRef](#)]
15. Zhang, X.; Huang, Y.-Y.; Cheng, J.-K.; Yao, Y.-G.; Zhang, J.; Wang, F. Alkaline earth metal ion doped Zn(II)-terephthalates. *CrystEngComm* **2012**, *14*, 4843. [[CrossRef](#)]
16. Burguert, B.; Klatt, G.; Gallego, D.; Tan, G.; Driess, M. Unprecedented silicon(II)→calcium complexes with N-heterocyclic silylenes. *Dalton Trans.* **2015**, *44*, 639–644. [[CrossRef](#)]
17. You, Z.; Wang, C.; Xiao, Y.; Guan, Q.; Li, J.; Xing, Y.; Gao, H.; Sun, L.; Bai, F. Integrated Photoresponsive Alkaline Earth Metal Coordination Networks: Synthesis, Topology, Photochromism and Photoluminescence Investigation. *Chem.-A Eur. J.* **2021**, *27*, 9605–9619. [[CrossRef](#)] [[PubMed](#)]
18. Finelli, A.; Héroult, N.; Crochet, A.; Fromm, K.M. Compartmentalization of Alkaline-Earth Metals in Salen-Type Cu- and Ni-Complexes in Solution and in the Solid State. *ACS Omega* **2019**, *4*, 10231–10242. [[CrossRef](#)]
19. Bo, Q.-B.; Zhang, Z.-W.; Miao, J.-L.; Wang, D.-Q.; Sun, G.-X. Novel metal–organic frameworks (MOFs) based on heterometallic nodes and 5-methylisophthalate linkers. *CrystEngComm* **2011**, *13*, 1765. [[CrossRef](#)]
20. Akine, S.; Taniguchi, T.; Saiki, T.; Nabeshima, T. Ca²⁺- and Ba²⁺-Selective Receptors Based on Site-Selective Transmetalation of Multinuclear Polyoxime–Zinc(II) Complexes. *J. Am. Chem. Soc.* **2005**, *127*, 540–541. [[CrossRef](#)]
21. Zou, R.; Zhong, R.; Han, S.; Xu, H.; Burrell, A.K.; Henson, N.; Cape, J.L.; Hickmott, D.D.; Timofeeva, T.V.; Larson, T.E.; et al. A Porous Metal–Organic Replica of α-PbO₂ for Capture of Nerve Agent Surrogate. *J. Am. Chem. Soc.* **2010**, *132*, 17996–17999. [[CrossRef](#)] [[PubMed](#)]
22. Ji, W.-J.; Liu, G.-F.; Wang, B.-Q.; Lu, W.-B.; Zhai, Q.-G. Design of a heterometallic Zn/Ca-MOF decorated with alkoxy groups on the pore surface exhibiting high fluorescence sensing performance for Fe³⁺ and Cr₂O₇²⁻. *CrystEngComm* **2020**, *22*, 4710–4715. [[CrossRef](#)]
23. Yang, D.-L.; Zhang, X.; Yao, Y.-G.; Zhang, J. Structure versatility of coordination polymers constructed from a semirigid ligand and polynuclear metal clusters. *CrystEngComm* **2014**, *16*, 8047–8057. [[CrossRef](#)]
24. Bo, Q.-B.; Wang, H.-Y.; Miao, J.-L.; Wang, D.-Q. Fluorescent Zn-based hetero-MOFs design via single metal site substitution. *RSC Adv.* **2012**, *2*, 11650. [[CrossRef](#)]
25. Liu, L.-L.; Yu, Y.-Z.; Zhao, X.-J.; Wang, Y.-R.; Cheng, F.-Y.; Zhang, M.-K.; Shu, J.-J.; Liu, L. A robust Zn(II)/Na(II)-MOF decorated with [(OAc)₂(H₂O)₂]_n²ⁿ⁻ anions for the luminescence sensing of copper ions based on the inner filter effect. *Dalton Trans.* **2018**, *47*, 7787–7794. [[CrossRef](#)] [[PubMed](#)]
26. Ma, L.; Du, P.; Yang, J.; Liu, Y.-Y.; Liu, X.-L.; Ma, J.-F. Two heterotrimetallic organic frameworks constructed using a functionalized Schiff base ligand: Syntheses, structures and visible photocatalytic activities for the degradation of chlorophenols. *RSC Adv.* **2016**, *6*, 98611–98619. [[CrossRef](#)]
27. Ejarque, D.; Calvet, T.; Font-Bardia, M.; Pons, J. Construction of Zn(II) Linear Trinuclear Secondary Building Units from A Coordination Polymer Based on α-Acetamidocinnamic Acid and 4-Phenylpyridine. *Molecules* **2020**, *25*, 3615. [[CrossRef](#)] [[PubMed](#)]
28. Ejarque, D.; Calvet, T.; Font-Bardia, M.; Pons, J. Amide-Driven Secondary Building Unit Structural Transformations between Zn(II) Coordination Polymers. *Cryst. Growth Des.* **2022**, *22*, 5012–5026. [[CrossRef](#)]

29. Mirosław, B.; Cristóvão, B.; Hnatejko, Z. Heterometallic Zn^{II}-Ln^{III}-Zn^{II} Schiff Base Complexes with Linear or Bent Conformation—Synthesis, Crystal Structures, Luminescent and Magnetic Characterization. *Molecules* **2018**, *23*, 1761. [[CrossRef](#)]
30. Chao, M.-Y.; Li, Q.; Zhang, W.-H.; Young, D.J. Metal-organic frameworks of linear trinuclear cluster secondary building units: Structures and applications. *Dalton Trans.* **2021**, *50*, 12692–12707. [[CrossRef](#)]
31. Mondal, S.; Dastidar, P. Designing Metallogelators Derived from NSAID-based Zn(II) Coordination Complexes for Drug-Delivery Applications. *Chem.-An Asian J.* **2020**, *15*, 3558–3567. [[CrossRef](#)] [[PubMed](#)]
32. Smolková, R.; Zeleňák, V.; Smolko, L.; Sabolová, D.; Kuchár, J.; Gyepes, R. Novel Zn(II) complexes with non-steroidal anti-inflammatory ligand, flufenamic acid: Characterization, topoisomerase I inhibition activity, DNA and HSA binding studies. *J. Inorg. Biochem.* **2017**, *177*, 143–158. [[CrossRef](#)] [[PubMed](#)]
33. Karmakar, A.; Sarma, R.J.; Baruah, J.B. Self-assembly of neutral dinuclear and trinuclear zinc-benzoate complexes. *Inorg. Chem. Commun.* **2006**, *9*, 1169–1172. [[CrossRef](#)]
34. Konidaris, K.F.; Kaplanis, M.; Raptopoulou, C.P.; Perlepes, S.P.; Manessi-Zoupa, E.; Katsoulakou, E. Dinuclear versus trinuclear complex formation in zinc(II) benzoate/pyridyl oxime chemistry depending on the position of the oxime group. *Polyhedron* **2009**, *28*, 3243–3250. [[CrossRef](#)]
35. Sheldrick, G.M. A short history of SHELX. *Acta Cryst. Sect. A* **2008**, *64*, 112–122. [[CrossRef](#)] [[PubMed](#)]
36. MacRae, C.F.; Sovago, I.; Cottrell, S.J.; Galek, P.T.A.; McCabe, P.; Pidcock, E.; Platings, M.; Shields, G.P.; Stevens, J.S.; Towler, M.; et al. Mercury 4.0: From visualization to analysis, design and prediction. *J. Appl. Cryst.* **2020**, *53*, 226–235. [[CrossRef](#)] [[PubMed](#)]
37. Persistence of Vision Pty. Ltd. *Persistence of Vision (TM) Raytracer*; Persistence of Vision Pty. Ltd.: Williamstown, Victoria, Australia, 2004.
38. Spek, A.L. Single-crystal structure validation with the program PLATON. *J. Appl. Cryst.* **2003**, *36*, 7–13. [[CrossRef](#)]
39. Llunell, M.; Casanova, D.; Cirera, J.; Alemany, P.; Alvarez, S. *SHAPE. Program for the Stereochemical Analysis of Molecular Fragments by Means of Continuous Shape Measures and Associated Tools*; Universitat de Barcelona: Barcelona, Spain, 2013.
40. Spackman, P.R.; Turner, M.J.; McKinnon, J.J.; Wolff, S.K.; Grimwood, D.J.; Jayatilaka, D.; Spackman, M.A. CrystalExplorer: A program for Hirshfeld surface analysis, visualization and quantitative analysis of molecular crystals. *J. Appl. Cryst.* **2021**, *54*, 1006–1011. [[CrossRef](#)]
41. Deacon, G.B.; Phillips, R.J. Relationships between the carbon-oxygen stretching frequencies of carboxylato complexes and the type of carboxylate coordination. *Coord. Chem. Rev.* **1980**, *33*, 227–250. [[CrossRef](#)]
42. Nakamoto, K. *Infrared and Raman Spectra of Inorganic and Coordination Compounds: Part A: Theory and Applications in Inorganic Chemistry*, 6th ed.; Wiley Interscience: Hoboken, NJ, USA, 2009.
43. Hadjiivanov, K.I.; Panayotov, D.A.; Mihaylov, M.Y.; Ivanova, E.Z.; Chakarova, K.K.; Andonova, S.M.; Drenchev, N.L. Power of Infrared and Raman Spectroscopies to Characterize Metal-Organic Frameworks and Investigate Their Interaction with Guest Molecules. *Chem. Rev.* **2021**, *121*, 1286–1424. [[CrossRef](#)]
44. Fleming, I.; Williams, D. *Spectroscopic Methods in Organic Chemistry*, 7th ed.; Springer International Publishing: Cham, Switzerland, 2019.
45. Pinsky, M.; Avnir, D. Continuous Symmetry Measures. 5. The Classical Polyhedra. *Inorg. Chem.* **1998**, *37*, 5575–5582. [[CrossRef](#)] [[PubMed](#)]
46. Yang, L.; Powell, D.R.; Houser, R.P. Structural variation in copper(I) complexes with pyridylmethylamide ligands: Structural analysis with a new four-coordinate geometry index, τ_4 . *Dalton Trans.* **2007**, 955–964. [[CrossRef](#)]
47. Morse, P.M.; Girolami, G.S. Are d⁰ ML₆ Complexes Always Octahedral? The X-ray Structure of Trigonal-Prismatic [Li(tmed)]₂[ZrMe₆]. *J. Am. Chem. Soc.* **1989**, *111*, 4114–4116. [[CrossRef](#)]
48. Friese, J.C.; Krol, A.; Puke, C.; Kirschbaum, K.; Giolando, D.M. Trigonal prismatic vs octahedral coordination geometry: Syntheses and structural characterization of hexakis (arythiolato) zirconate complexes. *Inorg. Chem.* **2000**, *39*, 1496–1500. [[CrossRef](#)] [[PubMed](#)]
49. Zhang, E.; Hou, H.; Meng, X.; Liu, Y.; Liu, Y.; Fan, Y. Ferrocenyl Functional Coordination Polymers Based on Mono-, Bi-, and Heterotrinnuclear Organometallic Building Blocks: Syntheses, Structures, and Properties. *Cryst. Growth Des.* **2009**, *9*, 903–913. [[CrossRef](#)]
50. Noh, K.; Ko, N.; Park, H.J.; Park, S.; Kim, J. Two porous metal-organic frameworks containing zinc-calcium clusters and calcium cluster chains. *CrystEngComm* **2014**, *16*, 8664–8668. [[CrossRef](#)]
51. Desiraju, G.R. Supramolecular Synthons in Crystal Engineering—A New Organic Synthesis. *Angew. Chem. Int. Ed. Engl.* **1995**, *34*, 2311–2327. [[CrossRef](#)]
52. Spackman, M.A.; McKinnon, J.J. Fingerprinting intermolecular interactions in molecular crystals. *CrystEngComm* **2002**, *4*, 378–392. [[CrossRef](#)]
53. Clegg, W.; Hunt, P.A.; Straughan, B.P.; Mendiola, M.A. Preparation and Characterisation of Linear Mixed-metal Trinuclear Carboxylate Complexes of General Formula [M₂M'(O₂CR)₆(C₉H₇N)₂]; Crystal Structure of [Zn₂Ba(O₂CCMe₃)₆]. *J. Chem. Soc. Dalton Trans.* **1989**, 1127–1131. [[CrossRef](#)]
54. Rubtsova, I.K.; Melnikov, S.N.; Shmelev, M.A.; Nikolaevskii, S.A.; Yakushev, I.A.; Voronina, J.K.; Barabanova, E.D.; Kiskin, M.A.; Sidorov, A.A.; Eremenko, I.L. Facile synthesis and structure elucidation of metal-organic frameworks with {ZnCa} and {Zn₂Ca} metal cores. *Mendeleev Commun.* **2020**, *30*, 722–724. [[CrossRef](#)]

55. Lemoine, P.; Viossat, B.; Dung, N.H.; Tomas, A.; Morgant, G.; Greenaway, F.T.; Sorenson, J.R.J. Synthesis, crystal structures, and anti-convulsant activities of ternary [ZnII(3,5-diisopropylsalicylate)2], [ZnII(salicylate)2] and [ZnII(aspirinate)2] complexes. *J. Inorg. Biochem.* **2004**, *98*, 1734–1749. [[CrossRef](#)] [[PubMed](#)]
56. Clegg, W.; Harbron, D.R.; Straughan, B.P. Structures of the mixed-metal carboxylate base adducts [MgZn₂(crotonate)₆(4-vinylpyridine)₂] and [MgCo₂(crotonate)₆(4-vinylpyridine)₄]. *Acta Cryst.* **1991**, *C47*, 267–270. [[CrossRef](#)]
57. Guo, L.; Liu, Y.; Guo, L.; Cao, J.; Li, W.; Liu, T.; Qiao, S.; Wang, B. A new porous heterometallic metal-organic framework for gas adsorption and luminescence sensing. *Z. Für Anorg. Und Allg. Chem.* **2021**, *647*, 1077–1082. [[CrossRef](#)]
58. Kang, X.-P.; Zhu, L.-H.; Hu, Y.-S.; An, Z. Organically templated (3,8)-connected microporous heterometallic Zn(II)–Sr(II) coordination polymer. *Inorg. Chem. Commun.* **2013**, *29*, 11–13. [[CrossRef](#)]
59. Clegg, W.; Little, I.R.; Straughan, B.P. Zinc Carboxylate Complexes: Structural Characterization of the Mixed-Metal Linear Trinuclear Complexes MZn₂(crot)₆(base)₂ (M = Mn, Co, Ni, Zn, Cd, Mg, Ca, Sr; crot[−] = Crotonate(1-); Base = Quinoline, 6-Methylqui. *Inorg. Chem.* **1988**, *27*, 1916–1923. [[CrossRef](#)]
60. Ma, L.-F.; Li, B.; Sun, X.-Y.; Wang, L.-Y.; Fan, Y.-T. Hydrothermal Syntheses and Characterizations of Three Zn^{II} Coordination Polymers Tuned by pH Value and Base. *Z. Für Anorg. Und Allg. Chem.* **2010**, *636*, 1606–1611. [[CrossRef](#)]
61. Rajak, R.; Saraf, M.; Mobin, S.M. Robust heterostructures of a bimetallic sodium–zinc metal–organic framework and reduced graphene oxide for high-performance supercapacitors. *J. Mater. Chem. A* **2019**, *7*, 1725–1736. [[CrossRef](#)]
62. Zhou, Y.-H.; Zhou, X.-W.; Zhou, S.-R.; Tian, Y.-P.; Wu, J.-Y. A series of coordination polymers constructed from R-isophthalic acid (R=−SO₃H, −NO₂, and −OH) and N-donor ligands: Syntheses, structures and fluorescence properties. *J. Solid State Chem.* **2017**, *245*, 190–199. [[CrossRef](#)]
63. Pramanik, A.; Fronczek, F.R.; Venkatraman, R.; Hossain, M.A. Hexa-μ-acetato-1:2κ⁴O,O';1:2κ²O:O;2:3κ⁴O,O';2:3κ²O:O-bis(4,4'-dimethyl-2,2'-bipyridine)-1κ²N,N';3κ²N,N'-2-calcium-1,3-dizinc. *Acta Cryst.* **2013**, *E69*, m643–m644. [[CrossRef](#)]
64. Wu, Z.-F.; Huang, X.-Y. A series of Mg–Zn heterometallic coordination polymers: Synthesis, characterization, and fluorescence sensing for Fe³⁺, CS₂, and nitroaromatic compounds. *Dalton Trans.* **2017**, *46*, 12597–12604. [[CrossRef](#)]
65. Chen, H.; Fan, L.; Hu, T.; Zhang, X. 6s-3d {Ba₃Zn₄}–Organic Framework as an Effective Heterogeneous Catalyst for Chemical Fixation of CO₂ and Knoevenagel Condensation Reaction. *Inorg. Chem.* **2021**, *60*, 3384–3392. [[CrossRef](#)] [[PubMed](#)]
66. Lakowicz, J.R. Introduction to Fluorescence. In *Principles of Fluorescence Spectroscopy*; Lakowicz, J.R., Ed.; Springer: Boston, MA, USA, 2009; pp. 1–26. ISBN 978-1-4020-9002-8.
67. Zhu, H.-B.; Zhao, J.; Kong, F.; Gou, S.-H.; Sun, Y.-M. Isostructural zinc (II) and cadmium (II) coordination complexes with 4-pyridin-4-yl-pyrimidine-2-sulfonate: Structure and fluorescent properties. *J. Mol. Struct.* **2009**, *928*, 95–98. [[CrossRef](#)]
68. Alessi, P.J.; Carter, E.C.; Fairchild, M.D.; Hunt, R.W.G.; McCamy, C.S.; Kráncz, B.; Moore, J.R.; Morren, L.; Noobs, J.H.; Ohno, Y.; et al. *CIE 15: Technical Report: Colorimetry*, 3rd ed.; Carter, E.C., Ohno, Y., Pointer, M.R., Robertson, A.R., Sève, R., Schanda, J.D., Witt, K., Eds.; International Commission on Illumination: Washington, DC, USA, 2004; ISBN 3-901-906-33-9.
69. Song, Y.; Wang, B.; Liu, Y.; Guo, L.-J.; Cao, J.-J.; Li, W.-H.; Liu, T.; Qiao, S.; Guo, L.-D. Heterometallic trinuclear cluster-based microporous metal-organic framework with high adsorption selectivity of CO₂ over N₂. *Inorg. Chem. Commun.* **2020**, *121*, 108202. [[CrossRef](#)]
70. Necefoglu, H.; Clegg, W.; Scott, A.J. A linear trinuclear CaZn₂ complex with bridging benzoate ligands. *Acta Cryst. Sect. E* **2002**, *58*, m123–m124. [[CrossRef](#)]
71. Cui, Y.; Zhang, X.; Zheng, F.; Ren, J.; Chen, G.; Qian, Y.; Huang, J. Two mixed-metal carboxylate–base adducts. *Acta Cryst.* **2000**, *C56*, 1198–1200. [[CrossRef](#)]
72. Escobedo-Martínez, C.; Lozada, M.C.; Gnecco, D.; Enriquez, R.G.; Soriano-García, M.; Reynolds, W.F. Acetate Bridged Trinuclear Zn, Ca and Mg Metal Complexes with 2- and 4-Substituted Pyridines. *J. Chem. Crystallogr.* **2012**, *42*, 794–802. [[CrossRef](#)]
73. Zhao, Y.-N.; Zhang, S.-R.; Wang, W.; Xu, Y.-H.; Che, G.-B. A 3D metal–organic framework with dual-aerial-octahedral trinucleate building units: Synthesis, structure and fluorescence sensing properties. *New J. Chem.* **2018**, *42*, 14648–14654. [[CrossRef](#)]
74. Gao, H.; Lou, X.; Li, Q.-T.; Du, W.-J.; Xu, C. Three new coordination polymers based on tripodal flexible ligand: Synthesis, structures and luminescent properties. *Inorg. Chim. Acta* **2014**, *412*, 46–51. [[CrossRef](#)]
75. Hazra, S.; Das, L.K.; Bhattacharya, R.; Drew, M.G.B.; Ghosh, A. Variations of structures on changing the ratios of metal ions in rare Ca(II)–Zn(II) hetero-metallic self-assembled coordination polymers of hexamethylenetetramine and benzoate. *J. Indian Chem. Soc.* **2021**, *98*, 100097. [[CrossRef](#)]